PAPER

Modeling and identification of nonlinear hysteresis behavior of piezoelectric actuators using a computationally efficient phenomenological model and modified cuckoo search algorithm

To cite this article: Xingyang Xie *et al* 2023 *Smart Mater. Struct.* **32** 015013

IOP Publishing Smart Materials and Structures
Smart Mater. Struct. **32** (2023) 015013 (18pp) https://doi.org/10.1088/1361-665X/aca7a5

Modeling and identification of nonlinear hysteresis behavior of piezoelectric actuators using a computationally efficient phenomenological model and modified cuckoo search algorithm

Xingyang Xie[1,2], **Yuguo Cui**[1,*], **Yang Yu**[3,*] **and Pan Chen**[1]

[1] Faculty of Mechanical Engineering & Mechanics, Ningbo University, Ningbo, Zhejiang, People's Republic of China
[2] Taizhou Customs Comprehensive Technical Service Center, Taizhou, Zhejiang, People's Republic of China
[3] Centre for Infrastructure Engineering and Safety, University of New South Wales, Sydney, NSW, Australia

E-mail: cuiyuguo@nbu.edu.cn and yang.yu12@unsw.edu.au

Received 8 June 2022, revised 26 November 2022
Accepted for publication 30 November 2022
Published 14 December 2022

Abstract

Hysteresis, an intrinsic characteristic of piezoelectric (PZT) actuators, has been demonstrated to dramatically reduce the capability and stability of the system. This paper proposes a novel computationally efficient model to describe nonlinear and hysteresis behaviors of PZT actuators. First of all, the model parameters are analyzed to investigate their effects on the output response. Then, a modified cuckoo search algorithm is used to identify the model parameters, without falling into the local optimum problems through introducing adaptive egg discovery probability and step length control factor. Further, the performance of the proposed model is validated using experimental data, via the comparison with classical Bouc-Wen and Prandtl-Ishlinskii hysteresis models. Finally, the rate-dependence of the parameters of proposed model is analyzed, which contributes to a generalized hysteresis model for the compensation control application of PZT actuators.

Keywords: piezoelectric (PZT) actuators, hysteresis modeling, computationally efficient phenomenological model, cuckoo search algorithm

(Some figures may appear in colour only in the online journal)

1. Introduction

Piezoelectric (PZT) actuators have been widely implemented for many years in applications of micropositioning systems such as hard disk drives [1, 2], micromachining [3, 4] and micromechanics in electronic assemblies [5, 6] on account of nano-scale displacement accuracy, rapid response of frequency and high rigidity. However, the primary disadvantage of PZT applications is the presence of hysteresis associated with them. The absence of compensation for hysteresis will lead to control problems such as static errors and vibrations, and may even result in instability of the positioning system where closed-loop control is implemented [7]. To

* Authors to whom any correspondence should be addressed.

compromise the hysteresis effect in PZT actuators, model-based compensation strategies such as predictive control or pseudo-inverse control can be implemented. However, these aforementioned control approaches need a precise model that is capable of describing the hysteresis behavior.

In the past few years, a large number of studies have been conducted to develop the hysteresis models for PZT actuators. In general, related models are categorized into two groups: physical models and phenomenological models. Physical hysteresis models are developed from the physical fundamentals of hysteresis materials by means of relationships between empirical equations and physical parameters. However, it is extremely hard to build physical models because of complicated physics of real systems with nonlinear hysteresis [8]. Different from physical models, phenomenological hysteresis models employ numerical equations directly to characterize nonlinear input and output relationships of hysteresis, without regard to the natural physical properties. Accordingly, phenomenological models are extensively applied in nonlinear hysteresis modeling of PZT actuators, such as Preisach model [9–12], Maxwell slip model [13, 14], Prandtl-Ishlinskii (PI) model [15–17], Rayleigh model [18], Dahl model [19], Duhem model [20, 21], Jiles–Atherton (J–A) model [22], neural networks model [23], frictional model [24], Bouc-Wen (BW) model [25–27], etc. Xiao and Li [12] developed a modified inverse Preisach model to characterize hysteretic responses of PZT actuators at a wide frequency range, where μ-density functions and weights were optimized by fast Fourier transform to realize the online rate-dependent compensation of PZT hysteresis in real-time. Liu *et al* [14] designed an extended Maxwell-slip model for portraying hysteretic behavior of PZT actuators, which consists of a stiffness function and a saturation deformation function. Savoie and Shann [17] considered the asymmetry property and thermal effect on the displacement outputs of PZT actuator, and proposed an asymmetrically temperature-dependent PI model. Xu and Li [19] proposed a novel phenomenological model of PZT actuator with Dahl hysteresis, the parameter of which were identified using particle swarm optimization (PSO) algorithm. Gan *et al* [20] revised the Duhem model to portray rate-dependent hysteretic responses of PZT actuators, where the trigonometric function was included with nonlinear least square (LS)-based parameter identification. Son and Anh [23] utilized a back-propagation neural network to develop a feed-forward controller to compensate for the hysteresis responses of PZT actuator, the performance of which has been validated by experimental data. Gan and Zhang [26] devised a general BW model with relaxation function, which well illustrates rate-dependent hysteretic responses of PZT actuators. In addition, as classical friction models, LuGre friction model and Leuven model were also reported in [24] about hysteresis modeling of PZT actuators. The above models have their own advantages. Preisach model has high accuracy in simulating hysteresis of piezoelectric actuator, GMS model improves the accuracy of hysteresis curve simulation by increasing the number of elastic slider elements, and Duhem model can describe hysteresis of a series of smart materials. BW model is widely used in the simulation of hysteresis of magnetorheological (MR) dampers, structures, isolation devices and soil behavior.

However, the above models still have some shortcoming, such as too many model parameters, difficult to solve nonlinear differential equations, large amount of calculation, difficult to determine intermediate functions. For example, BW model can simulate various types of hysteresis behavior through different parameter settings. On the other side, the expression of BW model has highly nonlinear differential equations, as well as the accuracy of parameters identification affected by cumulative iterative errors, which brings some obstacles to its practical application. The PI model is also complex and not easy to evaluate, which may lead to a poor performance.

It can be noticed that several hysteresis models have been reported in literature in the field of Magnetorheological materials [28–31]. However, unlike the purpose of predicting dynamic behavior of displacement and voltage of PZT actuators, these hysteresis models are mainly focused on characterizing the nonlinear dynamic behavior between force and displacement of Magnetorheological materials. Due to different variables and fields, these hysteresis models may not be applied into characterizing the relationship between displacement and voltage of PZT actuators directly.

On the other side, after the mathematical expressions of hysteresis models are determined, parameter identification is still a challenging task that can affect the modeling accuracy. In essence, model parameter identification is an optimization process, where the optimization target is to minimize the errors between real outputs of PZT actuators and model predictions. Swarm evolutionary algorithms have been employed for model parameter identification of PZT actuators, such as PSO [32], genetic algorithm (GA) [33], artificial bee colony (ABC) algorithm [34, 35], etc. In [25], hybrid GA and PSO methods were employed to identify the parameters of BW model for hysteresis response characterization of PZT actuators. The similar work can also be found in [35], where ABC algorithm was used for the same task of interest. Because of the configuration complexity of model to be identified, these optimization methods are not conducive to finding globally optimal solution in the case of poorly chosen initial values of model parameters [28]. Additionally, *a priori* knowledge of the parameter ranges is required to gain faster convergence. Recently, a novel metaheuristic optimization algorithm, namely cuckoo search (CS) algorithm, was proposed based on breeding parasitic behavior of cuckoo [36]. Due to the unique benefits of random walking and balanced mixing, CS algorithms with various variants have been widely utilized in the application of engineering optimization, including routing [37, 38], fault diagnosis [39, 40], node localization [41, 42], scheduling [43, 44], power system [45, 46], etc. Senthil and Kannapiran [37] designed an energy-efficient multipath routing algorithm based on CS algorithm to prolong the network lifespan with minimum energy cost. Xiao *et al* [39] employed CS algorithm to optimize the connection weights and bias of back-propagation neural network for fault category classification of rolling bearing. Ali *et al* [45] proposed an improved CS algorithm that improves tracking speeding

with minimal output power oscillations. Relevant research has proved that the CS algorithm is superior to PSO and GA in terms of convergence and optimization accuracy, when resolving nonlinear optimization problems with high dimensions [47]. Hence, it can be considered as a potential tool for parameter identification of hysteresis models of PZT actuators.

This study put forwards a novel computationally efficient phenomenological model for portraying nonlinear and hysteretic responses of PZT actuators. First, to better apply this model in PZT actuator modeling, the influence of each parameter on the model output is investigated. Second, using the experimental data collected from a PZT actuator tested with various loading frequency and voltage conditions, the model parameters are identified based on modified CS algorithm, the process of which is to solve a globally minimal optimization problem with the addition of adaptive egg discovery probability and step length control factor. Then, a comparison is made between the proposed model and BW model as well as PI model. Compared to classical BW model and PI model of PZT actuator, the proposed model has fewer tunable parameters and excludes highly nonlinear differential equations in the expression. Finally, a generalized model is developed with rate-dependent parameters for the compensation control application of PZT actuators.

The main challenge of this study is to as far as possible to establish a hysteresis model that can precisely describe the hysteresis characteristics of PZT actuator, while avoiding great amount of computation and iteration error. The need of this study is that, on one hand, the hysteresis modeling of PZT actuators still has some shortcoming, such as too many model parameters, large amount of calculation, difficult to determine intermediate functions. On the other hand, other hysteresis models in other field, e.g. MR materials, may not be applied to PZT actuators directly, due to different variables and fields. The main contribution and benefits of this study include threefold: (a) a computationally efficient phenomenological model is introduced, which has been proven with higher accuracy than commonly used model for characterizing the relationship between displacement and voltage of PZT actuator; and (b) the developed modified CS algorithm is effective in identifying model parameters with globally optimal solutions; and (c) a generalized hysteresis model is developed for the compensation control application as open loop control.

2. Proposed computationally efficient phenomenological model

2.1. Proposed model

Due to its excellent simulation ability, BW model has been widely used in nonlinear hysteresis simulation of piezoelectric actuators. BW model adopts a nonlinear differential equation with specific parameters to simulate hysteresis, as shown in equations (1) and (2). Parameters α control the size of the hysteresis ring, β and γ control the shape of the hysteresis ring, and parameter N controls the sharpness of the hysteresis displacement output $z_h(t)$. By selecting appropriate undetermined parameters, hysteresis rings of various shapes and types can be obtained, which can simulate different hysteresis behaviors.

$$z_h(t) = k_0 u(t) + g(t) \tag{1}$$

$$\dot{g}(t) = \alpha \dot{u}(t) - \beta |\dot{u}(t)| |g(t)|^{n-1} g(t) - \gamma \dot{u}(t) |g(t)| \tag{2}$$

Although the BW model has been proved to be effective in characterizing nonlinear systems with various hysteresis shapes, the modeling identification is always challenging owing to highly nonlinear differential equations in the model expression. As is known, the differential equations are generally resolved by the Euler method or Runge–Kutta method in an iterative way. The calculation procedure is time-consuming and the accuracy of identified parameters is affected by the accumulated iterative errors. To address this problem, this study proposes a novel computationally efficient hysteresis model, with the expression in equation (3).

$$z_h(t) = k_0 u(t) + \alpha \dot{u}(t) + \beta \cdot \tanh(\gamma u(t)) \tag{3}$$

where k_0 is a parameter to represent the stiffness of system, α represents viscosity coefficient of system, and the parameters of β and γ are related to the shape of hysteresis loops. Among the equation, $k_0 u(t)$ determines the Max/Min displacement output of piezoelectric actuators, $\alpha \dot{u}(t)$ determines the size of hysteresis loop, $\beta \cdot \tanh(\gamma u(t))$ determines the fundamental hysteresis loop.

Apparently, in the proposed model, an element based on hyperbolic tangent function is employed to replace nonlinear differential equations in BW model. Through replacing the nonlinear differential equation with a hyperbolic tangent function, the proposed model features less undetermined parameters and computation, and avoids the errors caused by dealing with nonlinear differential equations, while preserving the ability to simulate hysteresis loops of various types.

2.2. Model parameter analysis

To make full use of the proposed model for controller design application, a numerical study is conducted to investigate the influences of different model parameters on the displacement output. Here, take a one degree-of-freedom PZT actuator system as a case, and reference parameters of proposed model are set as: $k_0 = 0.145$, $\alpha = -0.0001$, $\beta = 0.385$ and $\gamma = 526\,000$. Suppose a harmonic voltage excitation is applied to the PZT actuator, with the inputs as expressed in equation (4):

$$u(t) = V_a \cdot \sin(2\pi f_v t + \varphi_0) + V_a \tag{4}$$

where V_a denotes the amplitude of input voltage; f_v denotes the excitation frequency; φ_0 is the initial phase angle of voltage excitation. In this investigation, V_a, f_v and φ_0 are set to 20 V, 20 Hz and $-\pi/2$, respectively. The sampling frequency and duration are set to 1000 Hz and 0.05 s, so a complete cycle of data can be obtained for this numerical analysis. Figure 1 shows the input voltage signals that are used to drive the PZT actuator.

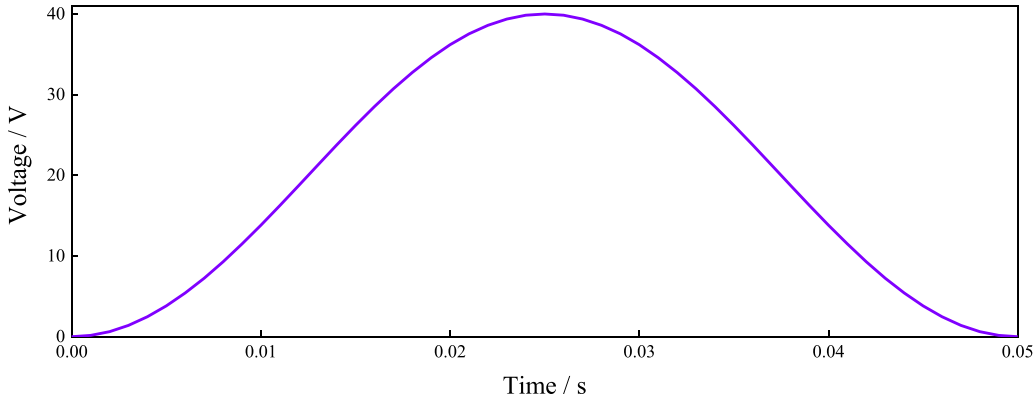

Figure 1. Input voltage signals in numerical investigation.

Then, each model parameter changes in a certain range from the reference value, while other parameters are set as reference values. Figure 2 portrays the hysteretic loops of the proposed model with different combinations of model parameters. Figure 2(a) shows the displacement outputs corresponding to different values of k_0 of 0.029, 0.087, 0.145, 0.203 and 0.261, which are 20%, 60%, 100%, 140% and 180% of reference value of k_0, respectively. Obviously, the maximum displacement output linearly ascends with the increase of k_0, since it indicates the stiffness of system, which is related to the slope of hysteresis loop. The influence of α on the hysteresis loop is illustrated in figure 2(b). Different from k_0, the change of α, representing viscosity ability of system, never affects the minimum and maximum displacement outputs. However, with the increase of α, the enclosed area expands continuously, which indicates the growing energy dissipation capability. Figure 2(c) depicts the hysteresis loops with different values of β. It is apparently seen that β has little influence on the response shape, including the width and shape of hysteresis loop. However, β is in proportion to the magnitude of output displacement. A high value of β contributes to a large displacement magnitude. Figure 2(d) explains the influence of γ on the displacement hysteresis loop, changes from 0, 50% 80%, 90% and 100% of the corresponding reference value, where only two scenarios can be observed from the analysis results. The main reason causing this result is that the hyperbolic tangent function achieves the upper and lower boundaries, when the absolute value of γ is above 2. Accordingly, it can be concluded that the main parameters contributing to the characteristics of hysteresis loop are k_0, α and β.

Besides the influences of model parameters(k_0, α, β and γ) on displacement outputs, the rate-dependent properties are also analyzed. Figure 2(e) shows the hysteresis responses under 40 Hz with voltages varying among 20, 40, 60 V. Figure 2(f) shows the hysteresis responses of model under frequencies varying among 20, 40, 60 Hz, with voltage staying 40 V. It is noted that compared with the effect of model parameters (k_0, α, β and γ), the input voltage and excitation frequency has much more influence on the enclosed hysteresis loops. With the increase of voltage amplitude and frequency, both slopes and enclosed areas of hysteresis loops significantly ascend.

3. Model parameter identification using modified CS algorithm

3.1. Modified CS algorithm

The CS algorithm was developed based on a simulation process of cuckoo breeding and egg-laying [36]. CS adopts the Lévy flight search method, which is a random walk satisfying a stable distribution of heavy tails in essence. The step length in CS alternates between short and long distances, which accordingly has the benefits of increasing the search space, expanding the population diversity and jumping out of the local optimum. To implement the CS algorithm, the following three idealized assumptions should be satisfied.

(a) Each cuckoo lays only one egg during each clutch, and randomly selects any host bird nest for incubation.
(b) Cuckoos satisfy the elite retention mechanism during the search, retaining the best host nest for the next generation.
(c) The nest number is fixed and the probability of cuckoos' eggs being found by the host bird is p. Once the host bird discovers that the eggs in the nest are not its own, it will discard the nest and find another location for a new nest. Therefore, the higher the value of p, the higher the probability that the nest will be discarded.

Similar to other swarm optimization algorithms, CS requires the generation of initial population, which is then updated using position iteration formula to generate new population and judged by iteration termination condition. If the termination condition is satisfied, the algorithm outputs the optimal solution, where the optimal position of the nest denotes a solution to the optimization objective. For an optimization problem with d-dimension, suppose the cuckoo swarm $X = [x_1, \ldots, x_d]$, and the cuckoo location is updated based on Lévy flight with the following equation:

$$X_i^{(t+1)} = X_i^{(t)} + \alpha sl \oplus L(\lambda)\ (i = 1, \ldots, N_{\text{pop}}, t = 1, \ldots, T_{\max}) \tag{5}$$

where $X_i^{(t+1)}$ and X_i^t denote the locations of ith cuckoo at the tth and $(t+1)$th iteration, respectively; t denotes the current

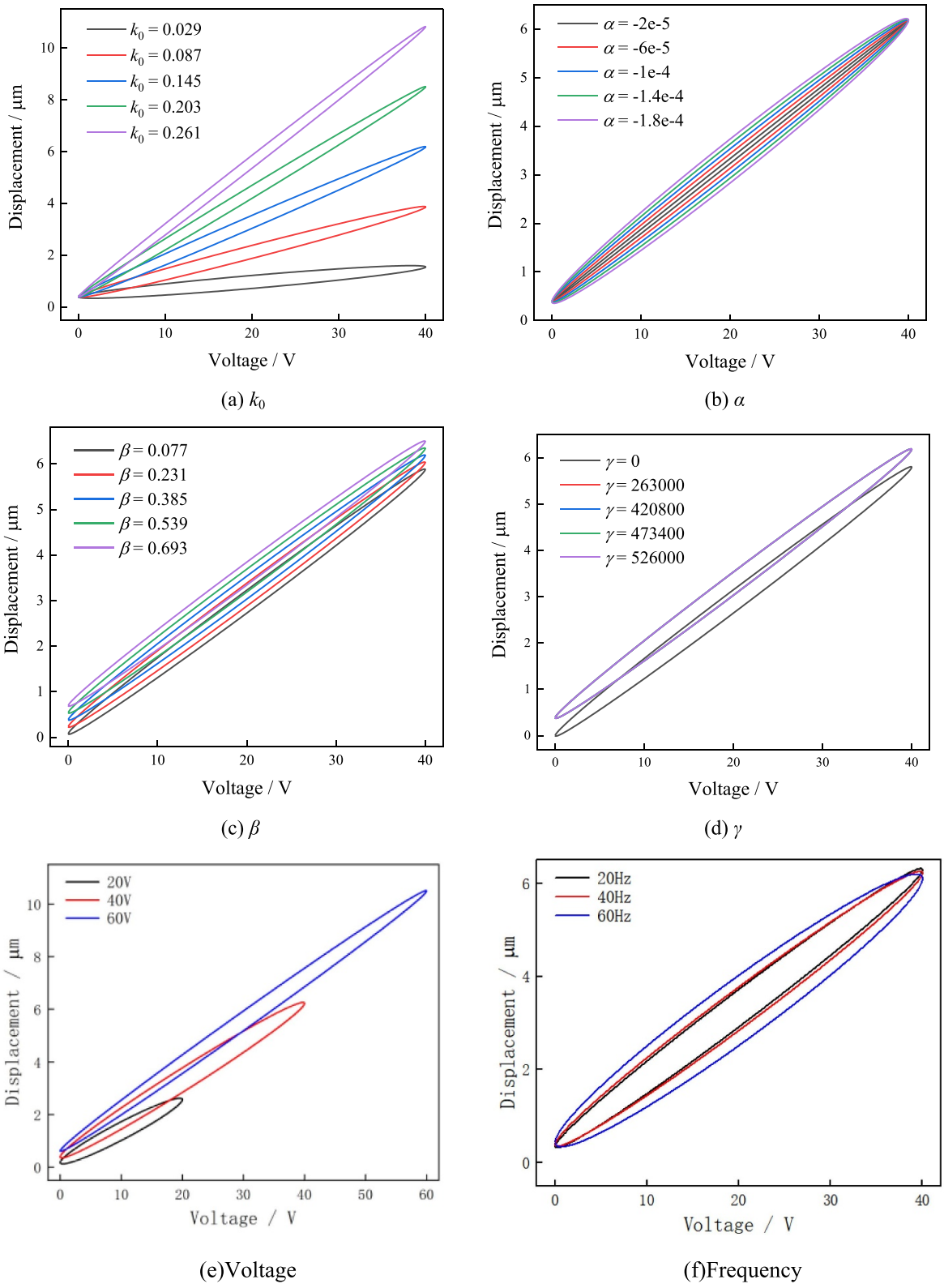

Figure 2. Influences of model parameters and input excitations on displacement outputs.

number of iteration; αsl denotes the step length control factor and generally $\alpha sl = 1$; N_{pop} denotes the swarm size; T_{max} is the maximum number of iterations; L is the Lévy flight step length, following the Lévy distribution, the expression of which is shown in equation (6).

$$L(\lambda) \sim u = t^{-\lambda}, 1 < \lambda < 3 \tag{6}$$

Equation (5) can be reformulated in the form below.

$$X_t^{(t+1)} = X_t^{(t)} + \alpha sl \frac{u}{v^{\frac{1}{\beta}}} \left[X_t^{(t)} - X_{best}^{(t)} \right] \tag{7}$$

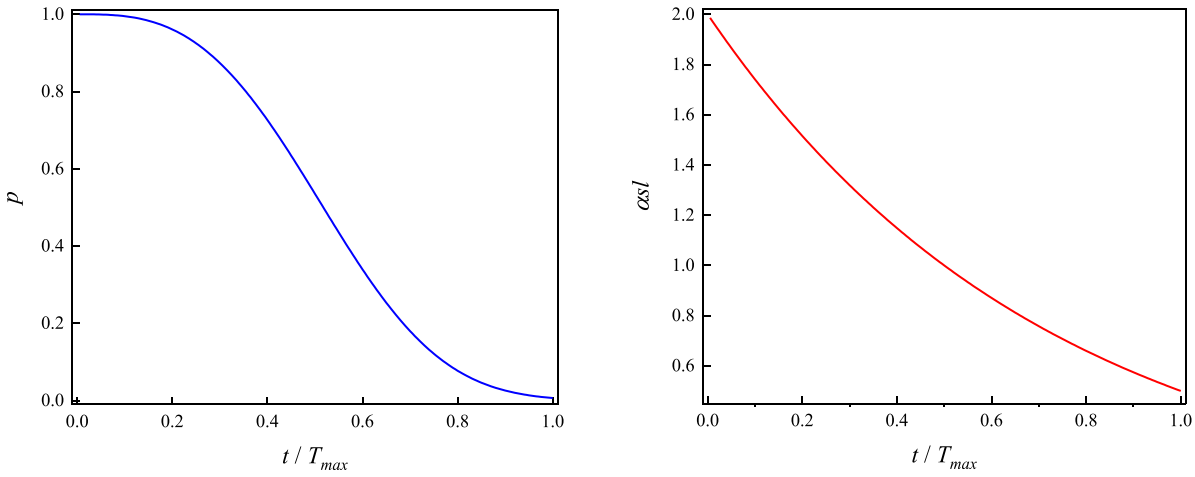

(a) Egg discovery probability (b) Step length control factor

Figure 3. Proposed adaptive parameters in modified CS.

where $X_{\text{best}}^{(t)}$ denotes the best location of cuckoos in the swarm at the tth iteration; β is a constant with the value between 1 and 2. u and v follow the normal distribution, i.e. $u \sim N\left(0, \sigma_u^2\right)$ and $v \sim N\left(0, \sigma_v^2\right)$, where σ_u^2 and σ_v^2 satisfy the following relationship.

$$\sigma_u^2 = \left\{ \frac{\Gamma(1+\beta)\sin\left(\frac{\pi\beta}{2}\right)}{\Gamma\left[\frac{1+\beta}{2}\right]\beta 2^{\frac{\beta-1}{2}}} \right\}, \sigma_v^2 = 1 \tag{8}$$

where Γ is the Gamma function, the probability distribution of which is unbounded in both variance and mean.

In the standard CS, the probability of the cuckoo's eggs being found p and the step length control factor αsl are always fixed during the evolutionary iteration procedure, which is insufficient for global search in the early stage of the iteration and also affects the local search capability of the algorithm in the later stage of iteration. Accordingly, the assignments of p and αsl are of great importance. Although the small values of p and αsl can enhance the local search ability of the algorithm, it will cause invalid iterations, which increase the calculation amount and affect the solution accuracy. Conversely, if p and αsl are assigned with large values, the algorithm may fall into the local optimum due to insufficient global search ability.

To address the aforementioned challenge in standard CS algorithm, this study proposes adaptive discovery probability of cuckoo's eggs and step length control factor to enhance the global search ability in the early stage and ensure the local search ability in the later stage. During the algorithm iteration procedure, the values of p and αsl dynamically change with the iteration number. The relevant expressions are provided in equations (9) and (10).

$$p(t) = p_{\min} + (p_{\max} - p_{\min}) \exp\left(-5\left(\frac{t}{T_{\max}}\right)^3\right) \tag{9}$$

$$asl(t) = asl_{\max} \exp\left(-\log\left(\frac{asl_{\max}}{asl_{\min}}\right)\frac{t}{T_{\max}}\right) \tag{10}$$

where $p_{\max}$ and $p_{\min}$ represent the maximum and minimum values of egg discovery probability of cuckoo, respectively; $asl_{\max}$ and $asl_{\min}$ represent the maximum and minimum values of step length control factor, respectively. In this study, $p_{\max} = 1, p_{\min} = 0, asl_{\max} = 2$ and $asl_{\min} = 0.5$, after a number of trials. Figure 3 displays the proposed egg discovery probability of cuckoo and step length control factor, respectively. It is clearly seen from the figure that the proposed adaptive egg discovery probability and step length control factor are capable of keeping larger values in the early stage of algorithm evolution to enhance the global search ability to avoid the algorithm from falling into the local optimum, and declining to small values in the later stage to guarantee the local search ability for improving the optimization accuracy. The procedure of the proposed modified CS algorithm can be summarized by the following steps, which is also presented in the flowchart in figure 4.

Step 1. Confirm the optimization objective, and initialize the parameters of modified CS algorithm, including the swarm optimization, maximum iteration number, fitness function, etc.

Step 2. Calculate the fitness value of each cuckoo's nest, and compare it with that of others to determine the optimal fitness $X_{\text{best}}^{(t)}$ in the swarm.

Step 3. Use equations (9) and (10) to update the egg discovery probability and step length control factor, and then use equation (7) to update the nest location of each cuckoo.

Step 4. Calculate the fitness values of new cuckoo nests, and find the optimal value, which is then compared with previous optimal value. If the current optimal value is better than previous one, update $X_{\text{best}}^{(t)}$. Otherwise, keep the optimal fitness unchanged.

Step 5. Generate a random number rand that is between 0 and 1, and compare rand with current p. If rand $> p$, randomly generated a new group of cuckoo nests. Otherwise, keep the nests unchanged and continue the iteration.

Step 6. Check the termination rule. In this study, the maximum iteration number $T_{\max}$ is used as the reference. If current iteration $t > T_{\max}$, stop the optimization and output the optimal solution. Otherwise, $t = t + 1$ go back to Step 3.

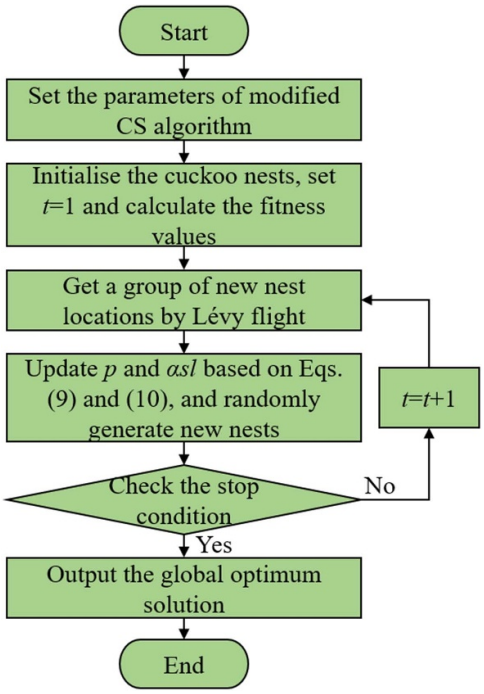

Figure 4. Flowchart of modified CS algorithm.

3.2. Parameter identification of proposed model using modified CS algorithm

In this research, based on the measured displacement-voltage responses in section 2, the parameters of the proposed computationally efficient hysteresis model of PZT actuator are identified by the newly developed modified CS algorithm, the procedure of which is to resolve a globally minimal optimization problem. The key to an optimization problem is to define a reasonable objective function, also known as fitness function. Here, the root mean square error (RMSE) between measured displacements and model predicted values in one sampling cycle is employed as the optimization target, with the mathematical formulation as follows.

$$\begin{aligned}\mathrm{RMSE} &= \frac{1}{N_{oc}}\sum_{N_{oc}}^{t=1}\left[z_h^{\mathrm{pred}}(t) - z_h^{\mathrm{exp}}(t)\right]^2 \\ &= \frac{1}{N_{oc}}\sum_{N_{oc}}^{t=1}\left[k_0 u(t) + \alpha\dot{u}(t) + \beta\cdot\tanh(\gamma u(t)) - z_h^{\mathrm{exp}}(t)\right]^2\end{aligned} \tag{11}$$

where N_{oc} denotes the sample number in one sampling frequency. For different excitation frequencies, the values of N_{oc} are different. z_h^{exp} and z_h^{pre} are experimentally measured displacement and predicted displacement by the proposed model, respectively. Using modified CS algorithm to resolve the fitness function is an iterative procedure, as shown in figure 5, where the model parameters of k_0, α, β and γ are constantly updated to lower the RMSE value as small as possible. If the fitness value is close to 0, the corresponding solution is the optimal values of model parameters. Accordingly, the model parameter optimization problem can be formulated as

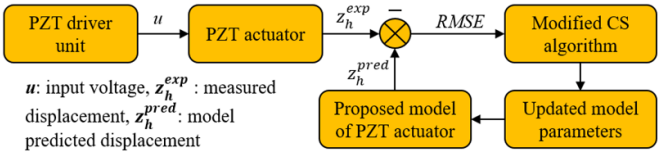

Figure 5. Schematic diagram of parameter identification of proposed model of PZT actuator.

$$\text{Min RMSE}\,(K_0, \alpha, \beta, \gamma) \tag{12}$$

4. Modeling verification and discussion

4.1. Experimental measurements of PZT displacement

The experimental setup for displacement measurement of PZT actuator is shown in figure 6. The experimental system consists of a computer, multifunctional data acquisition (DAQ) board card, PZT ceramic drive power supply, PZT actuator, drive unit, capacitive displacement sensor, auxiliary measurement bracket and 3D manual fine-tuning table. The measurement process is provided as follows: The multi-function DAQ board card converts the digital signal output by the computer into analog signal, which is output to the piezoelectric ceramic drive power supply. The output voltage of the drive power supply acts on the PZT actuator, and the drive unit produces micro displacement. The displacement can be measured by the capacitive non-contact displacement sensor, and finally the measured displacement is collected into the computer through the network port. Table 1 describes the instrument models and main parameters used in the experimental test system.

In order to deeply grasp the nonlinearly hysteretic characteristics of the PZT actuator, three types of sine wave voltages, namely 0–20 V-0, 0–40 V-0, 0–60 V-0, are applied to the PZT actuator in the drive unit, respectively. The excitation frequency ranges from 10 Hz to 80 Hz with the increment of 10 Hz, and the displacement output results were tested repeatedly. The corresponding hysteretic relationship between input voltage and output displacement can be obtained. For all the tests, the sampling duration is five excitation cycles for obtaining stable results. The voltage and displacement responses of the device can be obtained directly from the sensor readings, while the voltage change rate can be obtained via the differential calculation from time-voltage responses.

4.2. Modeling verification and analysis

Under each input voltage case, the parameters of the proposed computationally efficient hysteresis model of PZT actuator are identified by modified CS algorithm. To demonstrate the superiority of modified CS in model identification of PZT actuator, a comparison is conducted by comparing it with other heterogeneous swarm evolutionary optimization algorithms in terms of solution accuracy and convergence

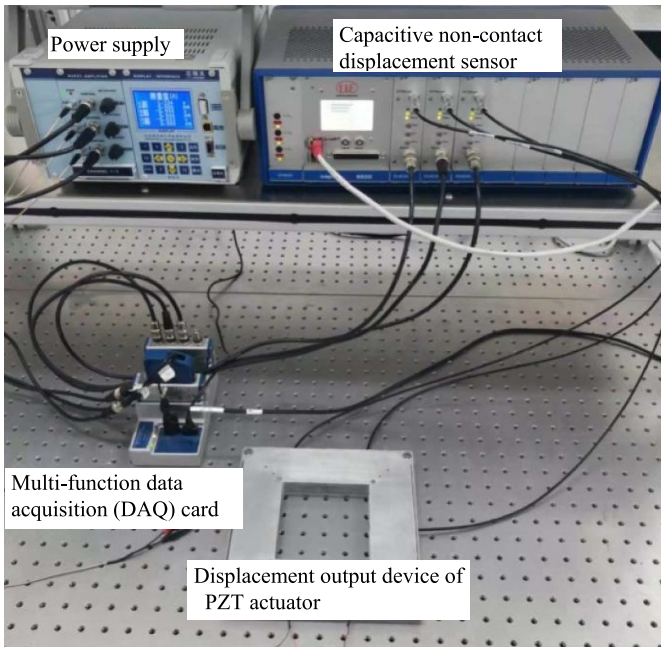

Figure 6. Displacement measurement system of PZT.

Table 1. Model and main parameters of the equipments.

Equipment	Model	Resolution	Sampling rate (kS/s/ch)
DAQ	NI 9263	16 bit	100
Piezoelectric actuator	XE501-C	16 bit	N/A
Capacitive sensor	CSE1	0.75 nm(2 Hz)/ 20 nm(8 kHz)	N/A

speed. The algorithms involved in this comparison include modified CS, standard CS and PSO, which are all implemented based on Matlab V2020b. The swarm size and maximum iteration number of standard CS and PSO are set the same as that of modified CS to undertake a fair evaluation, that is, $N_{\text{pop}} = 50$ and $T_{max} = 300$. For PSO, the inertia weight factor is linearly decreased with algorithm iteration, with the minimum and maximum values of 0.1 and 0.9, respectively; the acceleration coefficient is set to 1.5. Figure 7 shows the comparison of fitness performance of three algorithms to identify the parameters of proposed computationally efficient hysteresis model based on the experimental data case of 20 Hz frequency and 0–40 V-0 voltage. From the fitness iteration results, it is clearly seen that the fitness values gradually decline with the increase of iteration number. Among three algorithms, CS achieves the minimum value first and has the fastest convergence speed. However, it is premature due to lower solution accuracy compared to PSO and modified CS algorithms. Although modified CS has a slower convergence than PSO, it has the lowest fitness value among three algorithms, which indicates the best identification accuracy. The main reason causing the slower convergence in this case is perhaps owing to the proposed adaptive egg discovery probability and step length control factor, which improve the local search ability and keep the algorithm still fine-tuning the solution to obtain a higher accuracy at the later stage of iteration. Hence, it can be concluded that modified CS can be considered as an ideal tool for identifying the parameters of the proposed model of PZT actuators. Since there are eight excitation frequencies and three input voltage levels, there are a total of 24 groups of parameter combinations to be identified using modified CS algorithm, the results of which are summarized in tables 2–4, respectively.

To shorten representation space of simulation results, only hysteresis responses with frequencies of 10, 40, and 70 Hz are given in this paper. Figures 8(a)–10(a) compare the hysteresis responses of measured displacements and model predictions under the loading conditions of different frequencies in 10, 40, 70 Hz, with voltages varying among 20, 40, 60 V. It is noted that the excitation frequency has little influence on the enclosed hysteresis loops, which are mainly affected by the voltage level. With the increase of voltage level, both slopes and enclosed areas of hysteresis loops significantly ascend. The perfect matching between measured and predicted displacements sufficiently validates the capability of the proposed computationally efficient hysteresis model in characterizing hysteresis effect of PZT actuators. Figures 8(b)–10(b) analyze the model accuracy for each loading case by plotting the distributions of absolute errors between predicted results and real values. It is noticeable that all the cases have low mean values of absolute errors, representing high prediction accuracy. The standard deviations (Std) of prediction errors, however, increase with the adding maximum voltage. When the excitation voltage is 0–20 V-0, the absolute errors between real and predicted displacements are distributed in the range of −0.05–0.05; When the excitation voltage is 0–40 V-0, the absolute errors between real and predicted displacements are distributed in the range of −0.1–0.1; When the excitation voltage is 0–60 V-0, the absolute errors between real and predicted displacements are distributed in the range of −0.15–0.15. Overall, the prediction errors follow the normal distributions with satisfactory mean and Std results, which are acceptable in the modeling research.

To demonstrate the superiority of the proposed model over existing models in depicting the hysteresis responses of PZT actuators, a comparative study is conducted by comparison with commonly used BW model and PI model.

In BW model, it is worth noting that there is a highly nonlinear differential equation in the expression of BW model, as shown in equation (2), which increases the challenge in model parameter identification. In this study, the equation (2) is resolved using four-order Runge–Kutta method in an iterative manner. The detailed steps are demonstrated by equations (13)–(17).

$$f_1 = \Delta t \cdot \left[\alpha \dot{u}(t) - \gamma |\dot{u}(t)| |g(t)|^n - \beta |\dot{u}(t)| |g(t)|^{n-1} g(t)\right] \tag{13}$$

$$f_2 = \Delta t \cdot \left[\alpha \frac{(\dot{u}(t) + \dot{u}(t+1))}{2} - \gamma \left|\frac{\dot{u}(t) + \dot{u}(t+1)}{2}\right| \left|g(u) + \frac{f_1}{2}\right|^n - \beta \left|\frac{\dot{u}(t) + \dot{u}(t+1)}{2}\right| \left|g(t) + \frac{f_1}{2}\right|^{n-1} \left(g(t) + \frac{f_1}{2}\right)\right] \tag{14}$$

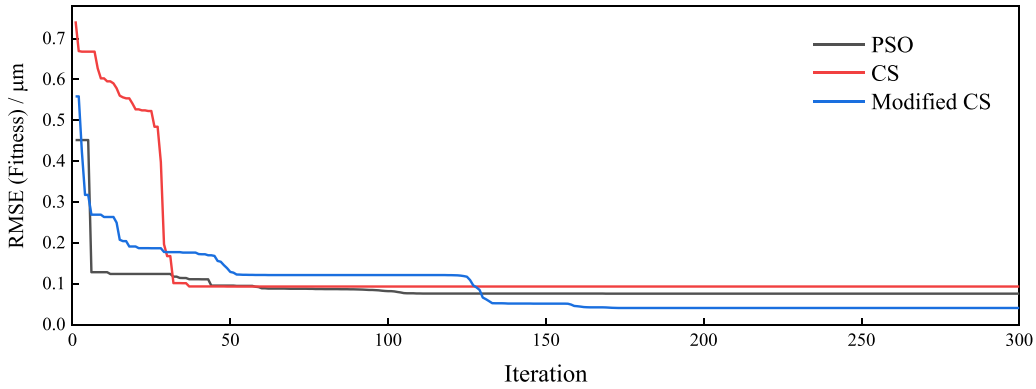

Figure 7. Fitness comparison of three optimization algorithms.

Table 2. Identification results of model parameters under the loading voltage case of 0–20 V-0.

Frequency	k_0	α	β	γ
10 Hz	0.1276	−4.5E-05	0.1228	47 918
20 Hz	0.1260	−6.1E-05	0.1285	41 276
30 Hz	0.1253	−3.0E-06	0.1363	49 162
40 Hz	0.1201	−1.4E-04	0.1734	44 419
50 Hz	0.1238	−1.2E-05	0.1475	16 536
60 Hz	0.1238	−7.0E-06	0.1431	29 944
70 Hz	0.1227	−3.9E-05	0.1387	47 111
80 Hz	0.1203	−5.9E-05	0.1623	36 141

Table 3. Identification results of model parameters under the loading voltage case of 0–40 V-0.

Frequency	k_0	α	β	γ
10 Hz	0.1517	−0.00017	0.3121	113 971
20 Hz	0.1487	−0.00016	0.3454	976 595
30 Hz	0.1482	−0.00006	0.3349	499 290
40 Hz	0.1461	−0.00009	0.3857	500 032
50 Hz	0.1447	−0.00009	0.4017	54 236
60 Hz	0.1424	−0.00010	0.4234	888 161
70 Hz	0.1397	−0.00010	0.4828	988 761
80 Hz	0.1451	−0.00003	0.4004	187 906

Table 4. Identification results of model parameters under the loading voltage case of 0–60 V-0.

Frequency	k_0	α	β	γ
10 Hz	0.1693	−0.00025	0.5189	401 360
20 Hz	0.1647	−0.00025	0.6521	863 764
30 Hz	0.1644	−0.00014	0.6248	1650 301
40 Hz	0.1647	−0.00005	0.6187	1709 695
50 Hz	0.1629	−0.00007	0.6436	1697 321
60 Hz	0.1628	−0.00005	0.6682	1350 147
70 Hz	0.1539	−0.00013	0.9466	1116 387
80 Hz	0.1600	−0.00007	0.7258	836 609

$$f_3 = \Delta t \cdot \left[\alpha \frac{(\dot{u}(t)+\dot{u}(t+1))}{2} - \gamma \left|\frac{\dot{u}(t)+\dot{u}(t+1)}{2}\right| \left|g(t)+\frac{f_2}{2}\right|^n - \beta \left|\frac{\dot{u}(t)+\dot{u}(t+1)}{2}\right| \left|g(t)+\frac{f_2}{2}\right|^{n-1} \left(g(t)+\frac{f_2}{2}\right)\right] \quad (15)$$

$$f_4 = \Delta t \cdot \left[\alpha \dot{u}(t+1) - \gamma |\dot{u}(t+1)| |g(t)+f_3|^n - \beta |\dot{u}(t+1)| |g(t)+f_3|^{n-1} (g(t)+f_3)\right] \quad (16)$$

$$g(t+1) = g(t) + \frac{[f_1 + 2(f_2+f_3) + f_4]}{6} \quad (17)$$

where Δt denotes the sampling time interval. In this research, $\Delta t = 0.000128$ s. To simplify the model expression and reduce the overall parameter number, n is set to 1 as suggested in [48]. Similarly, the fitness function of optimization problem for identifying the parameters of BW model is also defined as the RMSE between measured value and predicted value in one sampling cycle.

The PI model is composed of many basic hysteresis operators with different thresholds and has been proven effectively in improving the positioning accuracy of PZT actuators. In PI model, the basic operator is the play operator. The mathematical expression of the play operator is as follows:

$$y = \begin{cases} w_h(x - r_h), & x - \frac{y}{w_h} = r_h \\ c, & -r_h < x - \frac{y}{w_h} < -\frac{y}{w_h} \\ w_h(x + r_h), & x - \frac{y}{w_h} = -r_h \end{cases} \quad (18)$$

where, x and y are the input and output of the play operator respectively, r_h and w_h are the threshold and weight of the play operator respectively.

PI model can be constructed by weighted sum of play operators, as shown in equation (19).

$$y(t) = w_h^T \cdot H_r[x, y_0](t) = \sum_{i=0}^{n} H_r^i[x(t), y^i(0)] = \sum_{i=0}^{n} w_h^i \max\{x(t) - r_h^i, \min[x(t) + r_h^i, y^i(t-T)]\} \quad (19)$$

Figure 11 demonstrates the examples of comparison of model performance between proposed model and BW model as well as PI model in predicting displacement-voltage hysteresis loop of PZT actuator, where the load voltage is 0–40 V-0 and loading frequencies are 10 Hz and 30 Hz, respectively. From

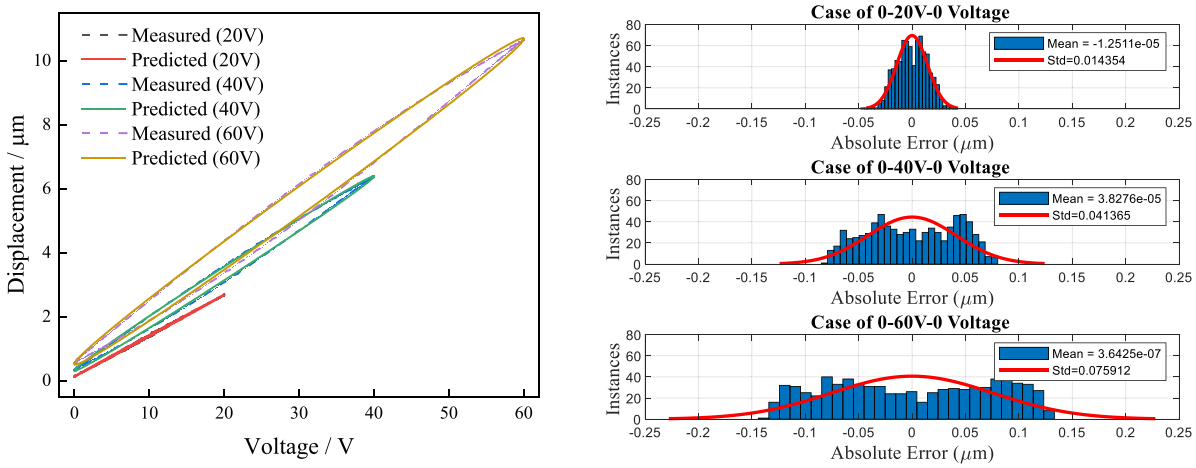

(a) Hysteresis responses (b) Error distributions

Figure 8. Modeling results and error analysis of 10 Hz frequency case.

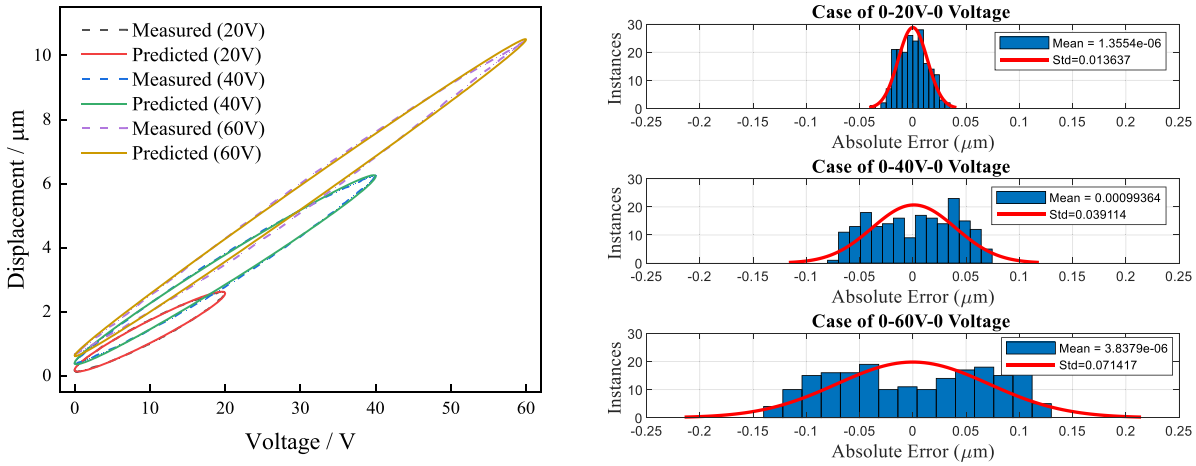

(a) Hysteresis responses (b) Error distributions

Figure 9. Modeling results and error analysis of 40 Hz frequency case.

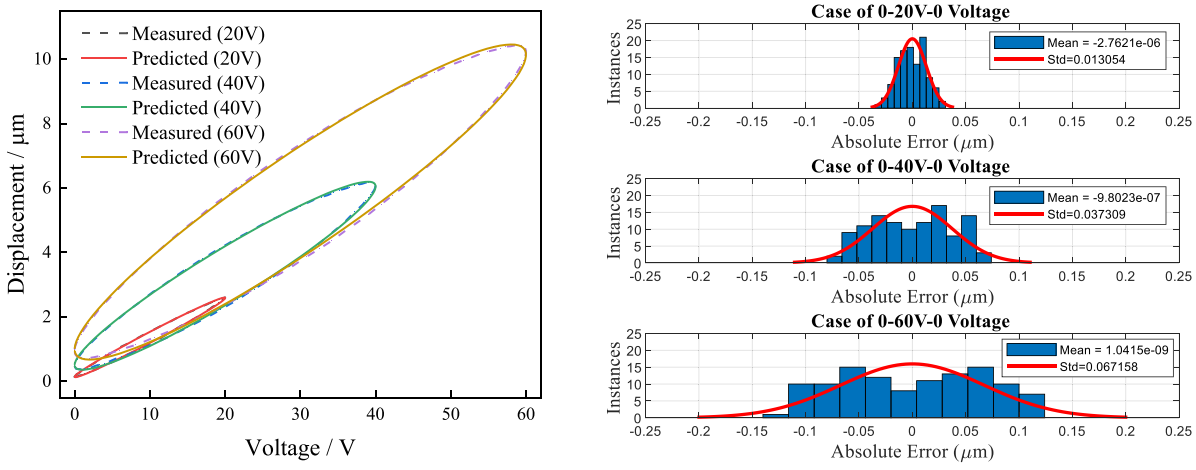

(a) Hysteresis responses (b) Error distributions

Figure 10. Modeling results and error analysis of 70 Hz frequency case.

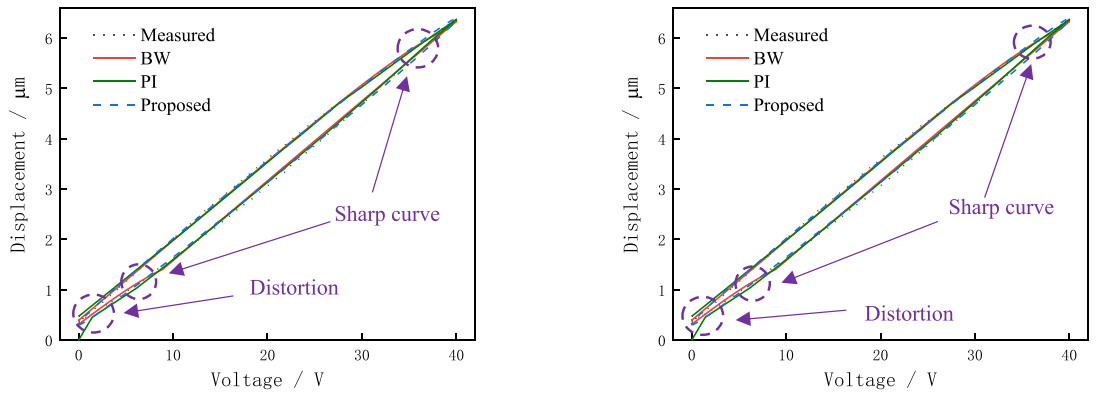

(a) Loading case of 0-40V-0 voltage and 10Hz frequency (b) Loading case of 0-40V-0 voltage and 30Hz frequency

Figure 11. Examples of hysteresis response comparison between proposed model and BW/PI models.

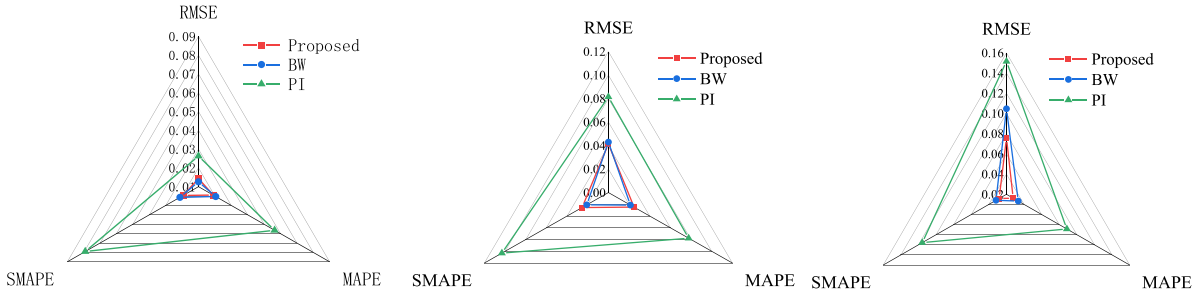

(a) 0-20V-0 voltage (b) 0-40V-0 voltage (c) 0-60V-0 voltage

Figure 12. Comparison of evaluation metrics between proposed model and BW/PI models for 10 Hz frequency case.

the results in figure 11, it is observed that the response predicted by the BW model has sharp curves (highlighted in the figures) because of the hysteresis represented by nonlinear differential equation, and the PI model also has sharp curves. Further, the PI model has obvious distortion when voltage get close to 0, and the hysteresis loop even cannot be closed, a poor performance when comparing to the proposed model and BW model. The proposed model, however, generates very smooth hysteresis loops, which is more in line with actual measurement. So, it has better fitting performance compared with BW and PI models.

To further prove the superiority of the proposed model, several commonly used statistical metrics are employed to comprehensively compare the performance of proposed model and commonly used models of PZT actuators, such as BW and PI models. Besides RMSE, mean absolute percentage error (MAPE) and symmetric MAPE (SMAPE) are also adopted in the model performance evaluation. For all three metrics, the lower the values of evaluation metrics, the better the model performance. The mathematical expressions of MAPE and SMAPE are given in equations (20) and (21).

$$\mathrm{MAPE} = \frac{1}{N_{oc}} \sum_{t=1}^{N_{oc}} \left| \frac{z_h^{\mathrm{pred}}(t) - z_h^{\exp}(t)}{z_h^{\exp}(t)} \right| \tag{20}$$

$$\mathrm{SMAPE} = \frac{1}{N_{oc}} \sum_{t=1}^{N_{oc}} \frac{\left| z_h^{\mathrm{pred}}(t) - z_h^{\exp}(t) \right|}{\left(z_h^{\mathrm{pred}}(t) + z_h^{\exp}(t) \right)/2}. \tag{21}$$

Similar to the simulation process, eight types of frequencies from 10 Hz to 80 Hz are applied to the PZT actuator in the drive unit respectively, with sine wave voltages namely 0–20 V-0, 0–40 V-0, 0–60 V-0. Through the calculation of equations (11), (20) and (21), RMSW, MAPE and SMAPE of BW/PI models and the proposed model can be obtained respectively. The performance comparison results of the three models in terms of RMSE, MAPE and SMAPE are displayed in figures 12–19, according to different excitation frequencies and voltage levels, in the form of radar plots. It can be seen from the results that the proposed model outperforms PI model in all excitation cases. Although BW model has a little bit better modeling performance in the excitation cases of (0–20 V-0, 10 Hz), (0–20 V-0, 40 Hz), (0–20 V-0, 50 Hz), (0–20 V-0, 60 Hz), (0–40 V-0, 10 Hz) and (0–40 V-0, 30 Hz), for other excitation cases, the proposed computationally efficient model has obvious advantages and higher capacity in modeling nonlinear and hysteretic displacement-voltage responses of PZT actuators. It can also be observed that when the excitation frequency and voltage level are low, the BW model is able to compete with the proposed model. However, with the

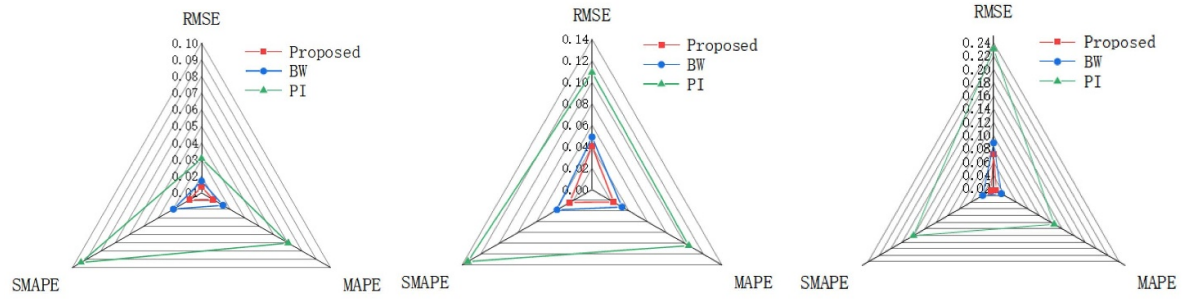

(a) 0-20V-0 voltage (b) 0-40V-0 voltage (c) 0-60V-0 voltage

Figure 13. Comparison of evaluation metrics between proposed model and BW/PI models for 20 Hz frequency case.

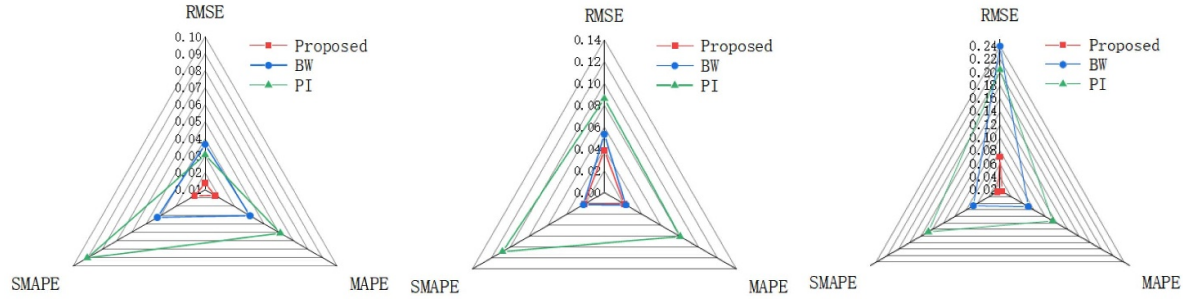

(a) 0-20V-0 voltage (b) 0-40V-0 voltage (c) 0-60V-0 voltage

Figure 14. Comparison of evaluation metrics between proposed model and BW/PI models for 30 Hz frequency case.

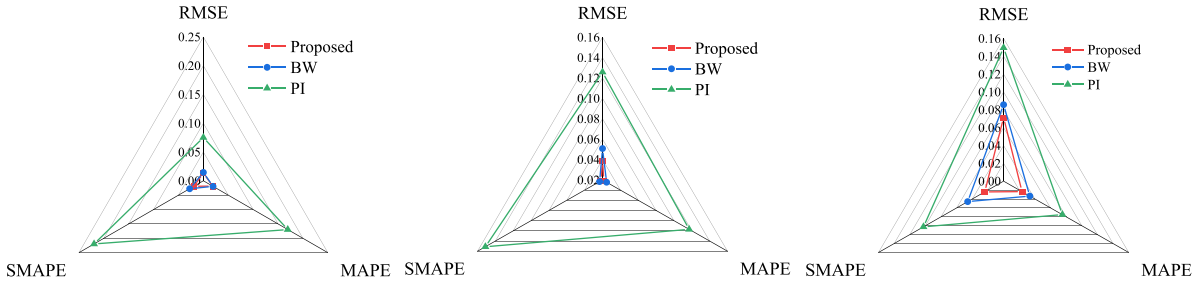

(a) 0-20V-0 voltage (b) 0-40V-0 voltage (c) 0-60V-0 voltage

Figure 15. Comparison of evaluation metrics between proposed model and BW/PI models for 40 Hz frequency case.

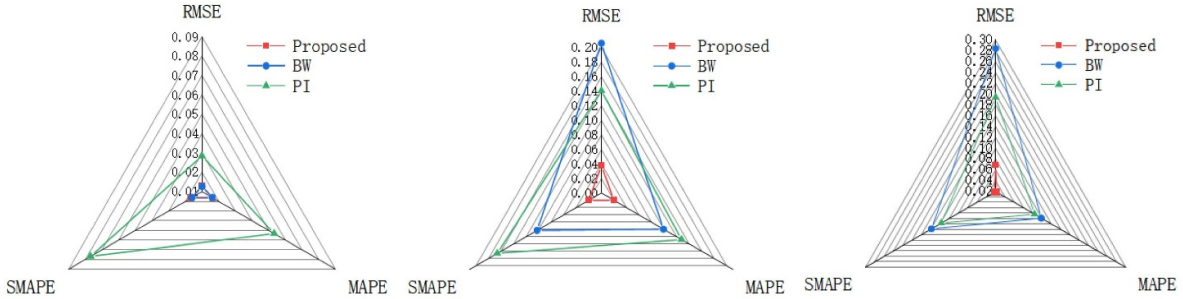

(a) 0-20V-0 voltage (b) 0-40V-0 voltage (c) 0-60V-0 voltage

Figure 16. Comparison of evaluation metrics between proposed model and BW/PI models for 50 Hz frequency case.

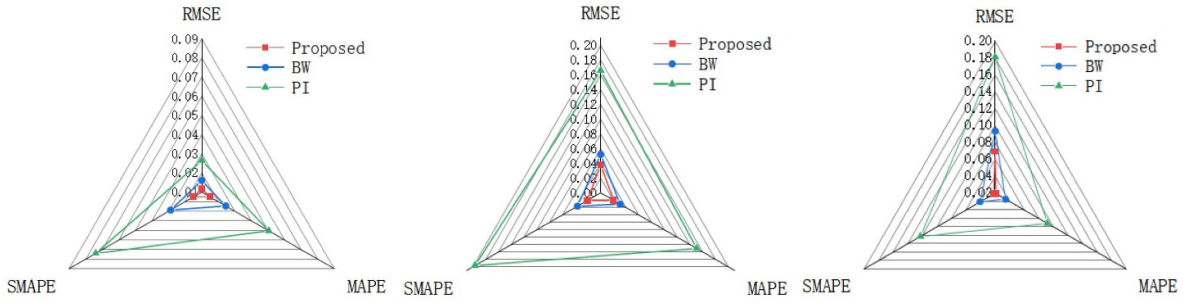

(a) 0-20V-0 voltage (b) 0-40V-0 voltage (c) 0-60V-0 voltage

Figure 17. Comparison of evaluation metrics between proposed model and BW/PI models for 60 Hz frequency case.

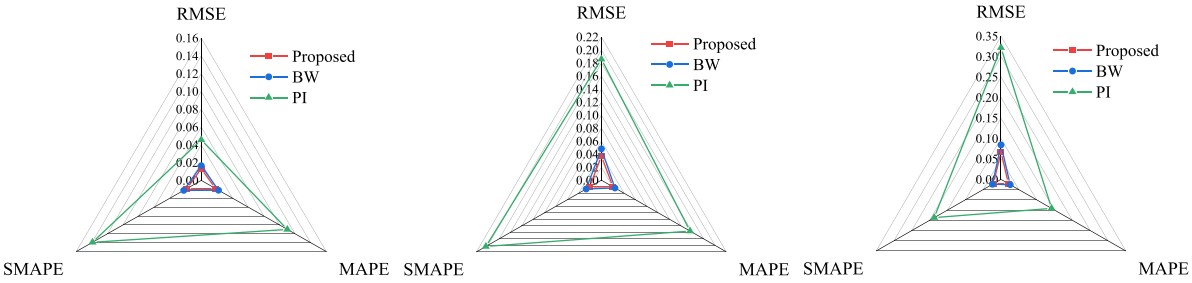

(a) 0-20V-0 voltage (b) 0-40V-0 voltage (c) 0-60V-0 voltage

Figure 18. Comparison of evaluation metrics between proposed model and BW/PI models for 70 Hz frequency case.

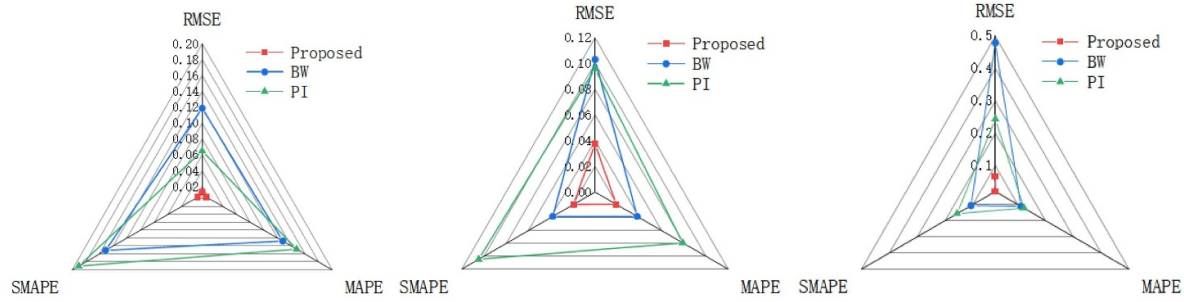

(a) 0-20V-0 voltage (b) 0-40V-0 voltage (c) 0-60V-0 voltage

Figure 19. Comparison of evaluation metrics between proposed model and BW/PI models for 80 Hz frequency case.

increase in excitation frequency and voltage level, the proposed model apparently outperforms the BW model for all the metrics. When the excitation level is 0–60 V-0, the values of RMSE, MAPE and SMAPE of the proposed model are 0.0759, 0.0276 and 0.0284 for 10 Hz frequency case, 0.0724, 0.0243 and 0.0248 for 20 Hz frequency case, 0.0713, 0.0240 and 0.0245 for 30 Hz frequency case, 0.0712, 0.0237 and 0.0241 for 40 Hz frequency case, 0.0693, 0.0227 and 0.0232 for 50 Hz frequency case, 0.0692, 0.0218 and 0.0222 for 60 Hz frequency case, 0.0669, 0.0208 and 0.0212 for 70 Hz frequency case, and 0.0673, 0.0213 and 0.0217 for 80 Hz frequency case. Under the same excitation voltage level, the relative errors of RMSE, MAPE and SMAPE between BW model and proposed model are 37.99%, 20.91% and 12.51% for 10 Hz frequency case, 41.02%, 30.83% and 22.66% for 20 Hz frequency case, 27.10%, 16.78% and 9.68% for 30 Hz frequency case, 20.28%, 41.68% and 90.72% for 40 Hz frequency case, 6.99%, 30.07% and 71.27% for 50 Hz frequency case, 7.62%, 20.58% and 54.14% for 60 Hz frequency case, 25.84%, 24.35% and 12.75% for 70 Hz frequency case, and 35.90%, 30.85% and 23.36% for 80 Hz frequency case. Accordingly, it can be concluded that the proposed computationally efficient model is comprehensively superior to the BW model in modeling PZT actuators.

Table 5. Comparison of running time.

Model		10 Hz	20 Hz	30 Hz	40 Hz	50 Hz	60 Hz	70 Hz	80 Hz
BW	Time (0–20 V-0)	0.5117	1.0874	1.0097	4.1312	15.5747	4.6794	11.8227	3.3361
	Time (0–40 V-0)	12.2657	3.9465	3.9665	5.2620	7.0465	10.0835	10.1817	6.0232
	Time (0–60 V-0)	5.5150	4.2252	4.9893	3.9041	25.9958	11.6945	11.7377	10.3886
PI	Time (0–20 V-0)	0.4688	0.5313	0.4219	0.7031	0.6406	0.5156	0.5938	0.5156
	Time (0–40 V-0)	0.6406	0.5625	0.625	0.6719	0.7031	0.5625	0.6406	0.5156
	Time (0–60 V-0)	0.5313	0.5938	0.5938	0.5156	0.7031	0.5469	0.7188	0.4063
Proposed	Time (0–20 V-0)	1.8323	1.0034	1.2134	3.1671	4.7374	2.3741	4.7264	2.3841
	Time (0–40 V-0)	3.4942	1.7363	2.3047	2.9831	5.3733	4.4947	5.9083	4.2938
	Time (0–60 V-0)	4.9383	1.8673	2.0173	1.3831	4.1383	4.3731	5.1662	5.3931

Table 6. Comparison of R-squared.

Model		10 Hz	20 Hz	30 Hz	40 Hz	50 Hz	60 Hz	70 Hz	80 Hz
BW	Time (0–20 V-0)	0.9998	0.9923	0.9984	0.9805	0.9998	0.9998	0.9943	0.9814
	Time (0–40 V-0)	0.9996	0.9972	0.9984	0.9951	0.9903	0.9802	0.9655	0.9975
	Time (0–60 V-0)	0.9991	0.9931	0.9956	0.9868	0.9936	0.9829	0.9095	0.9811
PI	Time (0–20 V-0)	0.9992	0.9989	0.999	0.9932	0.999	0.9992	0.9973	0.9947
	Time (0–40 V-0)	0.9986	0.9975	0.9984	0.9965	0.9957	0.994	0.9925	0.998
	Time (0–60 V-0)	0.9983	0.996	0.9968	0.9983	0.9971	0.9974	0.9921	0.9953
Proposed	Time (0–20 V-0)	0.9997	0.9997	0.9998	0.9998	0.9998	0.9998	0.9998	0.9998
	Time (0–40 V-0)	0.9995	0.9996	0.9996	0.9997	0.9997	0.9997	0.9997	0.9997
	Time (0–60 V-0)	0.9995	0.9996	0.9996	0.9996	0.9996	0.9996	0.9996	0.9996

Moreover, the running time of three different models for parameter identification is compared and summarized in table 5. It can be observed that the running time of the proposed model is less than that of classical BW model, due to without nonlinear differential equation in the model expression. Although PI is more efficient in model identification time than the proposed one, it has obvious problem of modeling accuracy. Accordingly, it can be concluded that the proposed computationally efficient model is comprehensively superior to the BW and PI models in modeling PZT actuators. Moreover, the R-squared of proposed model and BW/PI models is given in table 6. It can be observed that the proposed model outperforms BW/PI models.

4.3. Rate-dependence analysis for generalized hysteresis model

In the real application, the excitation frequency is unpredictable and needs more time to be modified, and thus the voltage seems a more available way to control the hysteresis results. To make full use of PZT actuators for control application, a voltage-dependent generalized model is developed to represent the relationship between input voltage and output displacement for the controller design. Here, the model parameter identification results in tables 2–4 are grouped according to different excitation voltage levels. For each voltage level, the model parameters of different excitation frequencies are averaged, and the averaged values, together with all the identified values, against voltage are depicted in figure 20. It is clearly seen from the results that the mean values of all four parameters have almost linear relationships with input voltage level, which can be represented by first-order polynomial functions, as shown in equations (22)–(26). For each expression, there are two unknown coefficients to be identified, and the identification procedure can be considered as resolving a linear LS problem, where parameter value and voltage level are deemed as constants for each case. Based on this method, the LS solutions of all the equations are obtained, as shown in table 7. As a result, a voltage-dependent generalized model is obtained with the expression in equation (26).

$$k_0(E) = k_{0,1} + k_{0,2} \cdot E \tag{22}$$

$$\alpha(E) = \alpha_1 + \alpha_2 \cdot E \tag{23}$$

$$\beta(E) = \beta_1 + \beta_2 \cdot E \tag{24}$$

$$\gamma(E) = \gamma_1 + \gamma_2 \cdot E \tag{25}$$

$$z_h(E,t) = k_0(E)\,u(t) + \alpha(E)\,\dot{u}(t) + \beta(E) \cdot \tanh\left(\gamma(E)\,u(t)\right) \tag{26}$$

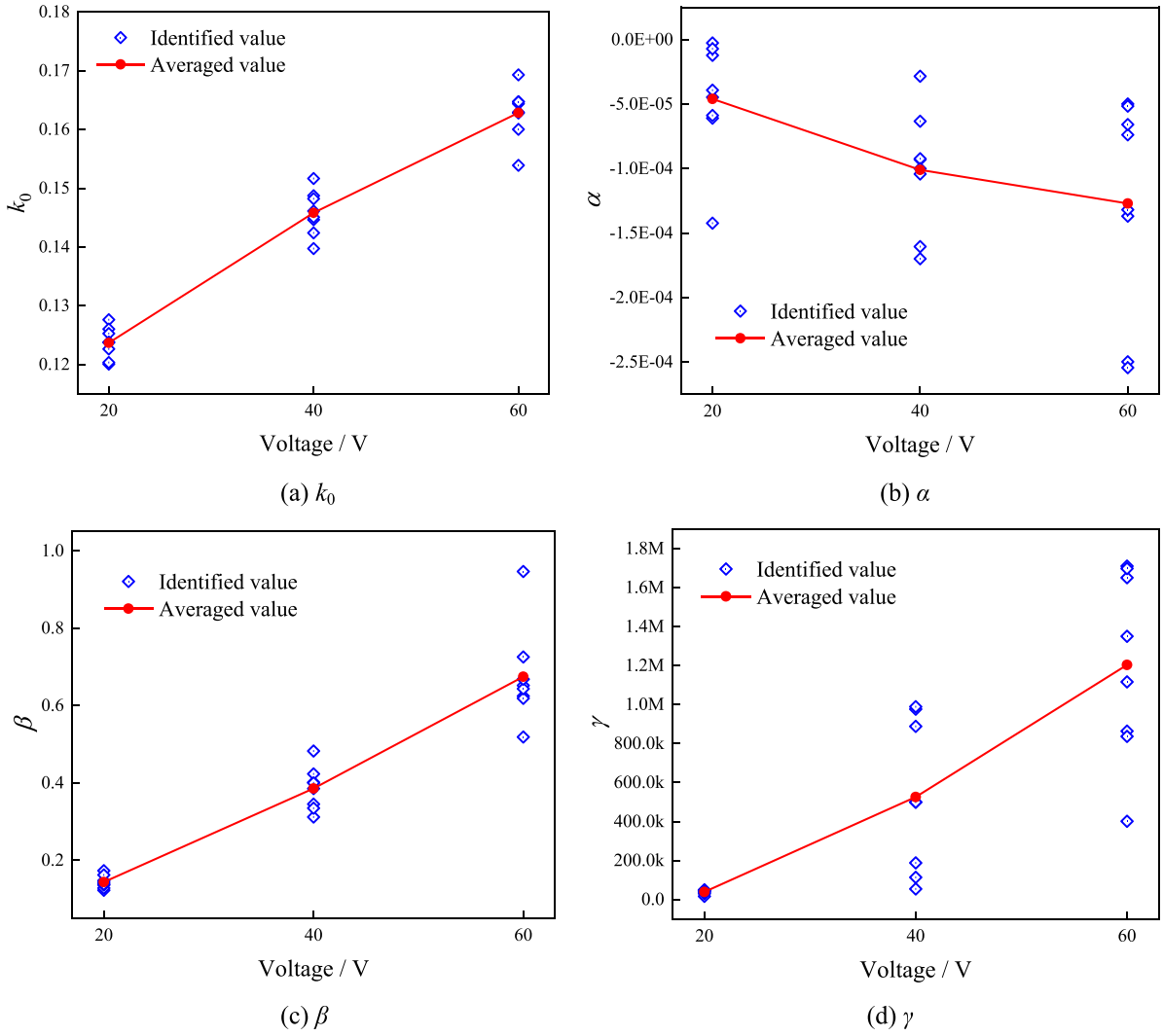

Figure 20. Relationships between averaged values of model parameters and input voltage level.

Table 7. Least square solutions to coefficients of polynomial functions of model parameters.

Parameter	Value	Parameter	Value
$k_{0,1}$ (μm V^{-1})	0.105	β_1	-0.1292
$k_{0,2}$ (μm V^{-2})	9.787e $-$ 04	β_2(1 V^{-1})	0.01327
α_1 (μm $\times$ s V^{-1})	-1.033e $-$ 05	(μm V^{-1})	-5.747e $+$ 05
α_2 (μm $\times$ s V^{-2})	-2.025e $-$ 06	γ_2(μm V^{-2})	2.91e $+$ 04

where E indicates the voltage level, which is in the range of [20–60] in this research.

To evaluate the performance of the rate-dependent generalized model, the experimental data are sent to equation (24) to get the displacement predictions, which are subsequently compared to measured displacements. Figure 21 shows the comparisons between measured displacements of PZT actuator and the displacements predicted by rate-dependent generalized model. The comparative results verify that the generalized model with rate-dependent parameters exhibits its excellent capability in modeling nonlinear response of PZT actuator, even if a few deviations occur at the peak-displacement areas. The promising result of good fitting also proves that the developed computationally efficient hysteresis model with rate-dependent parameters is an ideal candidate for the compensation control application of PZT transducers.

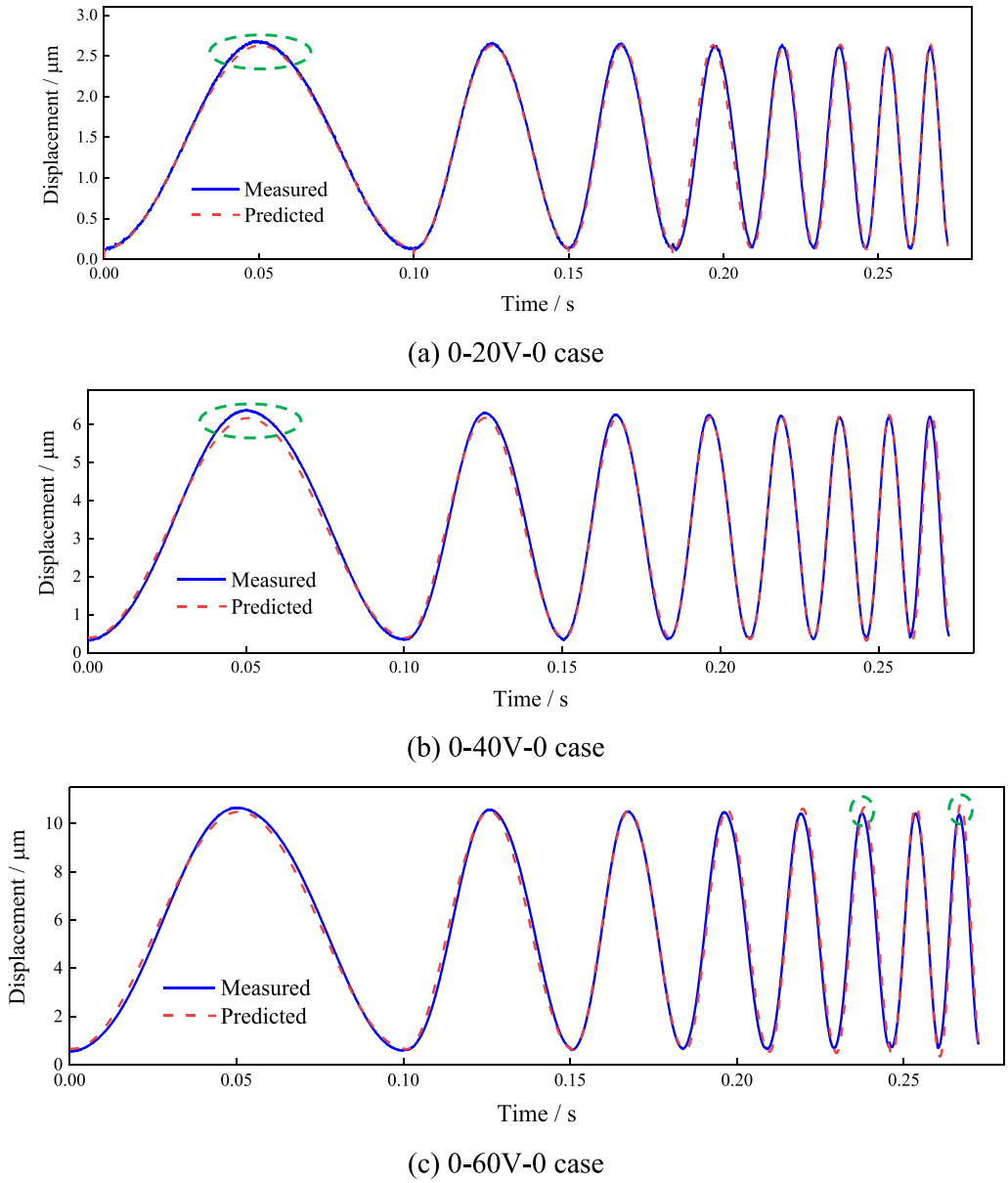

Figure 21. Time historical response comparisons between measured displacements and predictions from generalized model with rate-dependent parameters.

5. Conclusions

This study proposes a computationally efficient hysteresis model for characterizing nonlinear responses of PZT actuators. Compared to standard BW model that has been commonly used in hysteresis modeling, the proposed model has fewer parameters to be identified and excludes the nonlinear differential equation in the expression. A modified CS algorithm is then developed for parameter identification, the procedure of which is to resolve a globally minimal optimization problem. The performance of the proposed model and identification algorithm has been validated using the experimental data from the dynamic tests of a PZT actuator under various excitation conditions. The detailed conclusions are drawn as follows.

(a) The proposed computationally efficient hysteresis model is effective in depicting hysteresis displacement-voltage responses of PZT actuators with high accuracy and low prediction error.
(b) In the application of PZT actuator model identification, the proposed modified CS algorithm outperforms standard CS and PSO algorithms in the aspect of solution accuracy.
(c) The proposed computationally efficient hysteresis model is comprehensively superior to standard BW model for modeling PZT actuators, in terms of RMSE, MAPE and SMAPE.
(d) The rate-dependence of parameters of the proposed model is analyzed, which contributes to a generalized hysteretic model for the compensation control application.

In this study, for the control application, the average method was employed to calculate the mean values of all the model parameters under different excitation frequencies as the parameter values corresponding to the fixed voltage level. However, this method may generate a certain modeling error, since besides the voltage level, the excitation frequency also can affect the model parameters. Accordingly, in future work, the statistical distribution of each model parameter under different excitation frequencies will be considered for the controller design of PZT actuators. In addition, the hysteresis compensation control algorithm based on proposed model will be developed in future, the performance of which will be compared with controller based on other models for its practical application exploration. Moreover, the experimental conditions will be improved to enlarge actuating frequencies range of the experimental platform.

Data availability statement

The data that support the findings of this study are available upon reasonable request from the authors.

ORCID iDs

Yuguo Cui https://orcid.org/0000-0001-6636-4470
Yang Yu https://orcid.org/0000-0001-9592-8191

References

[1] Khasawneh Q A, Jaradat M A K, Naji M I and Al-Azzeh M Y 2018 Enhancement of hard disk drive manipulator using piezoelectric actuator mechanisms *J. Braz. Soc. Mech. Sci. Eng.* **40** 1–14
[2] Rahman M A, Al Mamun A and Yao K 2015 Rate dependent direct inverse hysteresis compensation of piezoelectric micro-actuator used in dual-stage hard disk drive head positioning system *Rev. Sci. Instrum.* **86** 085002
[3] Mohith S, Upadhya A R, Navin K P, Kulkarni S and Rao M 2020 Recent trends in piezoelectric actuators for precision motion and their applications: a review *Smart Mater. Struct.* **30** 013002
[4] Zhang B and Zhu Z 1997 Developing a linear piezomotor with nanometer resolution and high stiffness *IEEE/ASME Trans. Mechatronics* **2** 22–29
[5] Park J H, Yoshida K and Yokota S 1999 Resonantly driven piezoelectric micropump: fabrication of a micropump having high power density *Mechatronics* **9** 687–702
[6] Wang K, Wang D-H, Zhao J Y and Hou S 2021 A novel piezoelectric-actuated microgripper simultaneously integrated microassembly force, gripping force and jaw-displacement sensors: design, simulation and experimental investigation *Smart Mater. Struct.* **31** 015046
[7] Saleem A, Mesbah M and Shafiq M 2021 Feedback–feedforward control for high-speed trajectory tracking of an amplified piezoelectric actuator *Smart Mater. Struct.* **30** 025033
[8] Yu Y, Hoshyar A N, Li H, Zhang G and Wang W 2021 Nonlinear characterization of magnetorheological elastomer-based smart device for structural seismic mitigation *Int. J. Smart Nano Mater.* **12** 390–428
[9] Luo Y, Qu Y, Zhang Y, Xu M, Xie S and Zhang X 2019 Hysteretic modeling and simulation of a bilateral piezoelectric stack actuator based on Preisach model *Int. J. Appl. Electromagn. Mech.* **59** 271–80
[10] Nguyen P B, Choi S B and Song B K 2018 A new approach to hysteresis modelling for a piezoelectric actuator using Preisach model and recursive method with an application to open-loop position tracking control *Sens. Actuators* A **270** 136–52
[11] Pasco Y and Berry A 2004 A hybrid analytical/numerical model of piezoelectric stack actuators using a macroscopic nonlinear theory of ferroelectricity and a Preisach model of hysteresis *J. Intell. Mater. Syst. Struct.* **15** 375–86
[12] Xiao S and Li Y 2012 Modeling and high dynamic compensating the rate-dependent hysteresis of piezoelectric actuators via a novel modified inverse Preisach model *IEEE Trans. Control Syst. Technol.* **21** 1549–57
[13] Liu Y, Ni C, Du D and Qi N 2022 Learning piezoelectric actuator dynamics using a hybrid model based on Maxwell-slip and Gaussian processes *IEEE/ASME Trans. Mechatronics* **27** 725–32
[14] Liu Y, Du D, Qi N and Zhao J 2019 A distributed parameter Maxwell-slip model for the hysteresis in piezoelectric actuators *IEEE Trans. Ind. Electron.* **66** 7150–8
[15] Feng Y and Li Y 2021 System identification of micro piezoelectric actuators via rate-dependent Prandtl-Ishlinskii hysteresis model based on a modified PSO algorithm *IEEE Trans. Nanotechnol.* **20** 205–14
[16] Cheng L, Chen W and Tian L 2022 A modified direct inverse Prandtl-Ishlinskii model based on two sets of operators for the piezoelectric actuator hysteresis compensation *Int. J. Appl. Electromagn. Mech.* **68** 177–91
[17] Savoie M and Shan J 2022 Temperature-dependent asymmetric Prandtl-Ishlinskii hysteresis model for piezoelectric actuators *Smart Mater. Struct.* **31** 055022
[18] Zhang M and Damjanovic D 2020 A quasi-Rayleigh model for modeling hysteresis of piezoelectric actuators *Smart Mater. Struct.* **29** 075012
[19] Xu Q and Li Y 2010 Dahl model-based hysteresis compensation and precise positioning control of an XY parallel micromanipulator with piezoelectric actuation *J. Dyn. Syst. Meas. Control* **132** 041011
[20] Gan J, Mei Z, Chen X, Zhou Y and Ge M F 2019 A modified Duhem model for rate-dependent hysteresis behaviors *Micromachines* **10** 680
[21] Ji H, *et al* (ed) 2022 Modeling and control of hysteresis characteristics of piezoelectric micro-positioning platform based on Duhem model *Actuators* **11** 122
[22] Li Y, Zhu J, Li Y and Zhu L 2022 A hybrid Jiles–Atherton and Preisach model of dynamic magnetic hysteresis based on backpropagation neural networks *J. Magn. Magn. Mater.* **544** 168655
[23] Son N N and Anh H P H 2021 Hysteresis modelling and compensation for piezoelectric actuator using Jaya-BP neural network *Proc. Inst. Mech. Eng.* C **235** 7836–47
[24] Fung R F, Han C F and Chang J R 2008 Dynamic modeling of a high-precision self-moving stage with various frictional models *Appl. Math. Model.* **32** 1769–80
[25] Zhang Q, Dong Y, Peng Y, Luo J, Xie S and Pu H 2019 Asymmetric Bouc–Wen hysteresis modeling and inverse compensation for piezoelectric actuator via a genetic algorithm–based particle swarm optimization identification algorithm *J. Intell. Mater. Syst. Struct.* **30** 1263–75
[26] Gan J and Zhang X 2019 Nonlinear hysteresis modeling of piezoelectric actuators using a generalized Bouc–Wen model *Micromachines* **10** 183

[27] Wang D and Zhu W 2011 A phenomenological model for pre-stressed piezoelectric ceramic stack actuators *Smart Mater. Struct.* **20** 035018
[28] Yu Y, Yousefi A M, Yi K, Li J, Wang W and Zhou X 2021 A new hybrid model for MR elastomer device and parameter identification based on improved FOA *Smart Struct. Syst.* **28** 617–29
[29] Yu Y, Li Y, Li J, Gu X and Royel S J 2018 Nonlinear characterization of the MRE isolator using binary-coded discrete CSO and ELM *Int. J. Struct. Stab. Dyn.* **18** 1840007
[30] Yu Y, Li J, Li Y, Li S, Li H and Wang W J 2019 Comparative investigation of phenomenological modeling for hysteresis responses of magnetorheological elastomer devices *Int. J. Mol. Sci.* **20** 3216
[31] Wang T and Zhu Z-W 2021 A new type of nonlinear hysteretic model for magnetorheological elastomer and its application *Mater. Lett.* **301** 130176
[32] Yang M-J, Gu G-Y and Zhu L-M 2013 Parameter identification of the generalized Prandtl–Ishlinskii model for piezoelectric actuators using modified particle swarm optimization *Sens. Actuators* A **189** 254–65
[33] Gan J and Zhang X 2019 A review of nonlinear hysteresis modeling and control of piezoelectric actuators *AIP Adv.* **9** 040702
[34] Yang L, Zhao Z, Zhang Y and Li D 2021 Rate-dependent modeling of piezoelectric actuators for nano manipulation based on fractional Hammerstein model *Micromachines* **13** 42
[35] Wang G, Zhou K and Zhang Y 2018 Parameter identification of piezoelectric hysteresis model based on improved artificial bee colony algorithm *Mod. Phys. Lett.* B **32** 1850131
[36] Yang X S and Deb S (eds) 2009 Cuckoo search via Lévy flights *2009 World Congress on Nature and Biologically Inspire Computing (NaBIC)* (IEEE)
[37] Senthil T and Kannapiran B 2017 ECTMRA: energy conserving trustworthy multipath routing algorithm based on cuckoo search algorithm *Wirel. Pers. Commun.* **94** 2239–58
[38] SH G 2021 ZHRP-DCSEI, a novel hybrid routing protocol for mobile ad-hoc networks to optimize energy using dynamic cuckoo search algorithm *Wirel. Pers. Commun.* **118** 3289–301
[39] Xiao M, Liao Y, Bartos P, Filip M, Geng G and Jiang Z 2021 Fault diagnosis of rolling bearing based on back propagation neural network optimized by cuckoo search algorithm *Multimedia Tools and Applications* **81** pp 1567–87
[40] Cheng J, Wang L and Xiong Y 2019 Cuckoo search algorithm with memory and the vibrant fault diagnosis for hydroelectric generating unit *Eng. Comput.* **35** 687–702
[41] Kotiyal V, Singh A, Sharma S, Nagar J and Lee C-C 2021 ECS-NL: an enhanced cuckoo search algorithm for node localisation in wireless sensor networks *Sensors* **21** 3576
[42] Cheng J and Xia L 2016 An effective cuckoo search algorithm for node localization in wireless sensor network *Sensors* **16** 1390
[43] Zheyuan C, Hammid A T, Kareem A N, Jiang M, Mohammed M N and Kumar N M 2021 A rigid cuckoo search algorithm for solving short-term hydrothermal scheduling problem *Sustainability* **13** 4277
[44] Zhou B, Li X and Zhang Y 2021 Improved multi-objective cuckoo search algorithm with novel search strategies for point-to-point part feeding scheduling problems of automotive assembly lines *Assem. Autom.* **41** 24–44
[45] Ali E M, Abdelsalam A K, Youssef K H and Hossam-Eldin A A 2021 An enhanced cuckoo search algorithm fitting for photovoltaic systems' global maximum power point tracking under partial shading conditions *Energies* **14** 7210
[46] Eltamaly A M 2021 An improved cuckoo search algorithm for maximum power point tracking of photovoltaic systems under partial shading conditions *Energies* **14** 953
[47] Yang X-S and Deb S 2014 Cuckoo search: recent advances and applications *Neural Comput. Appl.* **24** 169–74
[48] Gan J and Zhang X 2018 An enhanced Bouc-Wen model for characterizing rate-dependent hysteresis of piezoelectric actuators *Rev. Sci. Instrum.* **89** 115002